



CHALMERS
UNIVERSITY OF TECHNOLOGY

Acidochromic Behaviors of Indacenodithiophene-Based Conjugated Polymers Containing Azo, Imine, and Vinyl Bonds

Downloaded from: <https://research.chalmers.se>, 2025-04-03 02:38 UTC

Citation for the original published paper (version of record):

Kotewicz, K., Franco, L., Araujo, M. et al (2025). Acidochromic Behaviors of Indacenodithiophene-Based Conjugated Polymers Containing Azo, Imine, and Vinyl Bonds. *Macromolecules*, 58(5): 2719-2729.
<http://dx.doi.org/10.1021/acs.macromol.4c02700>

N.B. When citing this work, cite the original published paper.

Acidochromic Behaviors of Indacenodithiophene-Based Conjugated Polymers Containing Azo, Imine, and Vinyl Bonds

Krzysztof Kotewicz, Leandro R. Franco, Moyses Araujo,* and Ergang Wang*



Cite This: *Macromolecules* 2025, 58, 2719–2729



Read Online

ACCESS |



Metrics & More

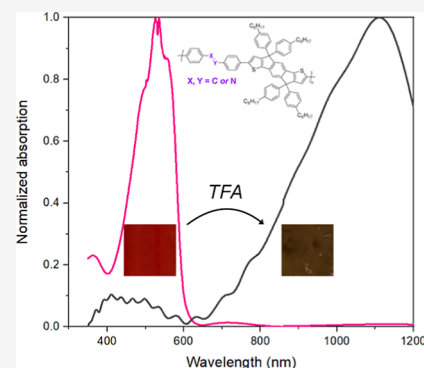


Article Recommendations



Supporting Information

ABSTRACT: Acidochromic materials possess significant potential for the development of molecular switches, acid sensors, smart displays, and erasable/reprintable media. The semiconductive nature of conjugated polymers exhibiting such a behavior makes them ideal for use in electronic devices. In this study, we present a comparative investigation of three indacenodithiophene-based conductive polymers, containing azo, imine, and vinyl bonds (namely, PIDT-BAB, PIDT-BIB, and PIDT-BVB, respectively). We examined the alterations in the spectral properties of these polymers upon exposure to trifluoroacetic acid (TFA). The acidochromic response of PIDT-BAB and PIDT-BIB is indicated by DFT calculations to occur via protonation at the nitrogen atom. PIDT-BIB demonstrated heightened sensitivity to TFA. Conversely, PIDT-BVB did not display acidochromic properties in the film but was responsive to TFA in solution through acid doping. Repeated exposure of polymer films was used to examine the robustness of the polymers over 50 cycles. DFT calculations showed an increase in the planarity of PIDT-BAB and PIDT-BIB backbones as a result of protonation. This effect was particularly strong in PIDT-BAB, resulting in an unusually large bathochromic shift of 510 nm. The corresponding pink-to-transparent transition is particularly interesting for applications in sensors. Our findings provide valuable guidelines for the design of conjugated polymers tailored for acidochromic devices.



1. INTRODUCTION

Materials exhibiting changes in their spectral properties in response to acids, i.e., acidochromism, have garnered considerable research attention. Proposed applications of acidochromic materials include among others fluorescent switches,^{1,2} organic display technologies,³ rewritable media,^{4,5} anticounterfeiting,^{6,7} chemical sensing,^{8,9} actuators,¹⁰ and integrated acidochromic organic photovoltaic device.¹¹ Numerous acidochromic compounds have been reported to date, based on different structures, such as pyridine,¹² quinoline,¹³ quinoxaline,¹⁴ diazene,¹⁵ imidazole,¹⁶ thiazole,¹⁷ and amines.¹⁸ The structures are mostly based on nitrogen-containing moieties, as their interactions with acids are almost exclusively occurring via protonation of nitrogen atoms.¹⁹ Moreover, absorption shifts reported for the small-molecule acidochromic materials are typically limited up to around 200 nm to further enlarge this shift from these materials could be challenging.^{6,8,17,20} Acidochromic behavior has been widely studied, with many well-established materials on the market, most notably standard laboratory pH papers. Food packaging is another area where many developments are made to monitor the spoilage of packaged products.²¹ However, direct implementation of acidochromic behavior into organic electronic devices is yet to be fulfilled.

Conjugated polymers have been the subject of intense scientific research in recent decades. Their alternating single–double bond backbone structure facilitates the delocalization of π -electrons over large polymer segments, enabling their

semiconductive properties. The resulting properties provide unique opportunities for a variety of applications, such as organic light-emitting diodes (OLED), light-emitting electrochemical cells (LECs), organic solar cells, transistors, sensors, and energy storage and biomedical devices.^{22–25} Conjugated polymers have also been investigated as acidochromic materials directly,^{26,27} or as a matrix for acidochromic small molecules,^{28,29} but their acidochromic mechanism and design principle have been rarely studied. Addressing this gap is important to enable optimal application of conjugated polymers in research on acidochromic materials.

Therefore, this study focuses on the synthesis and characterization of three new conjugated polymers bearing azo-, imine-, and vinyl-bond, respectively, with the intention of systematic study of their structure–property relationships and the exploration of their potential application as acidochromic sensors. The Stille coupling reaction was employed to polymerize IDT monomers with azo-, imine-, and vinyl-bond containing monomers, forming PIDT-BAB, PIDT-BIB, and PIDT-BVB, respectively. Azo dyes, being one of the most

Received: November 2, 2024

Revised: February 13, 2025

Accepted: February 18, 2025

Published: February 28, 2025



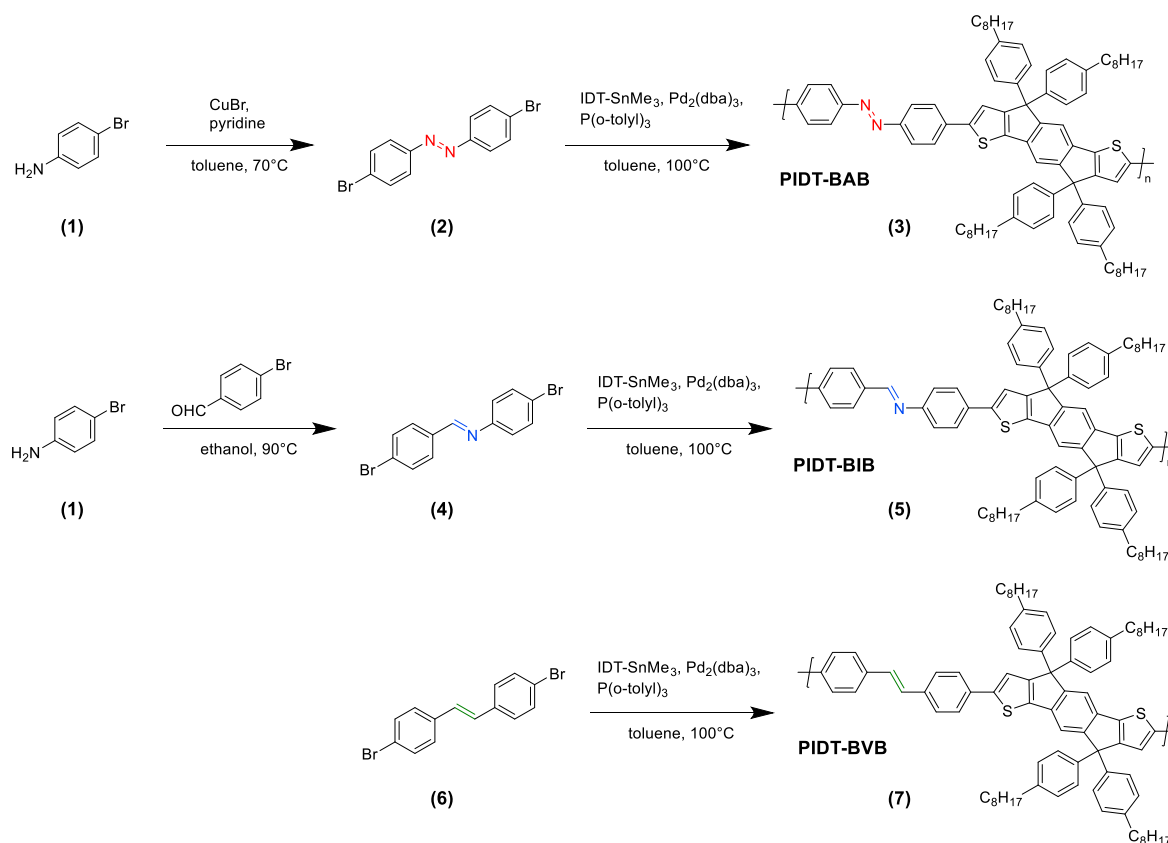


Figure 1. Synthesis route of PIDT-BAB, PIDT-BIB, and PIDT-BVB.

extensively utilized classes of dyes globally,³⁰ present an appealing choice for a chromophore, with the reported instances demonstrating their utility in acidochromic applications.^{17,31} Schiff bases containing the C=N bond have been used in acidochromic materials in particular as well.^{20,26,32} The vinyl bond containing the polymer was synthesized for comparison as a still fully conjugated polymer without nitrogen atoms in the backbone. The synthesized polymers were characterized by UV–vis absorption spectrometry in the film and solution. TFA was used to test the acidochromic response in UV–vis absorption spectrometry in solution. The reversibility of the process was examined by the cyclic exposure of polymer films to TFA and triethylamine (TEA) vapors. The polymers were characterized by cyclic voltammetry (CV) to determine their HOMO and LUMO energy levels. Density functional theory (DFT) calculations were carried out to shed light on how protonation and oxidation affect both the electronic structure of the ground state and the electronic transitions within the polymers. The results lead to the conclusion that both azo and imine bonds undergo protonation at the nitrogen atoms in the presence of TFA. An unprecedented superior bathochromic shift of 510 nm occurs in the absorption of PIDT-BAB upon protonation. This is contributed to the combination of protonation induced enhanced intramolecular charge transfer effect and accumulated effects of multiple monomer units. This significant shift is far beyond that of any acidochromic small molecules reported to our knowledge, highlighting the advantages of acidochromic polymers. Imine bond-containing PIDT-BIB in turn exhibits superior sensitivity to TFA, responding to TFA at 50 times lower concentration in chloroform solution compared with PIDT-BAB. Moreover, the PIDT-BIB films can universally

switch at exposure to various organic and inorganic acids. Another finding is that the PIDT-BVB's acidochromic response is the result of oxidation, rather than protonation.

2. RESULTS AND DISCUSSION

2.1. Polymer Design and Synthesis. For this study, a series of three conjugated polymers were chosen for investigation, each featuring a moiety of interest: an azo, imine, or vinyl bond. Monomers containing them were coupled with the same indacenodithiophene (IDT) comonomer resulting in the formation of PIDT-BAB, PIDT-BIB, and PIDT-BVB, respectively. IDT is a commonly used structural unit in the design of conjugated polymers.³³ Combining its electron-rich structure with the electron-poor azo- and imine-containing monomers results in a donor–acceptor motif, commonly implemented in organic electronics.³⁴ Long side chains of the IDT unit increase the solubility of the polymers. The overview of the synthetic pathway for the polymers is presented in Figure 1.

2.2. Optical Properties. UV–vis absorption spectra of PIDT-BAB, PIDT-BIB, and PIDT-BVB in chloroform solutions with a concentration of 0.01 mg·mL⁻¹ were collected before and after the addition of TFA. The recorded spectra are presented in Figure 2, along with pictures of the corresponding solutions. The spectra plotted in terms of energy are shown in Figure S2. The summary of the absorption properties is shown in Table 1. The optical band gaps were determined from Tauc plots³⁵ (Figure S1). The absorption maxima (λ_{\max}) of PIDT-BAB, PIDT-BIB, and PIDT-BVB were observed at 557, 484, and 495 nm, respectively. After the addition of TFA to the solutions, all absorption maxima exhibited bathochromic shifts to 1067, 667, and 631 nm, respectively. The largest shift of 510

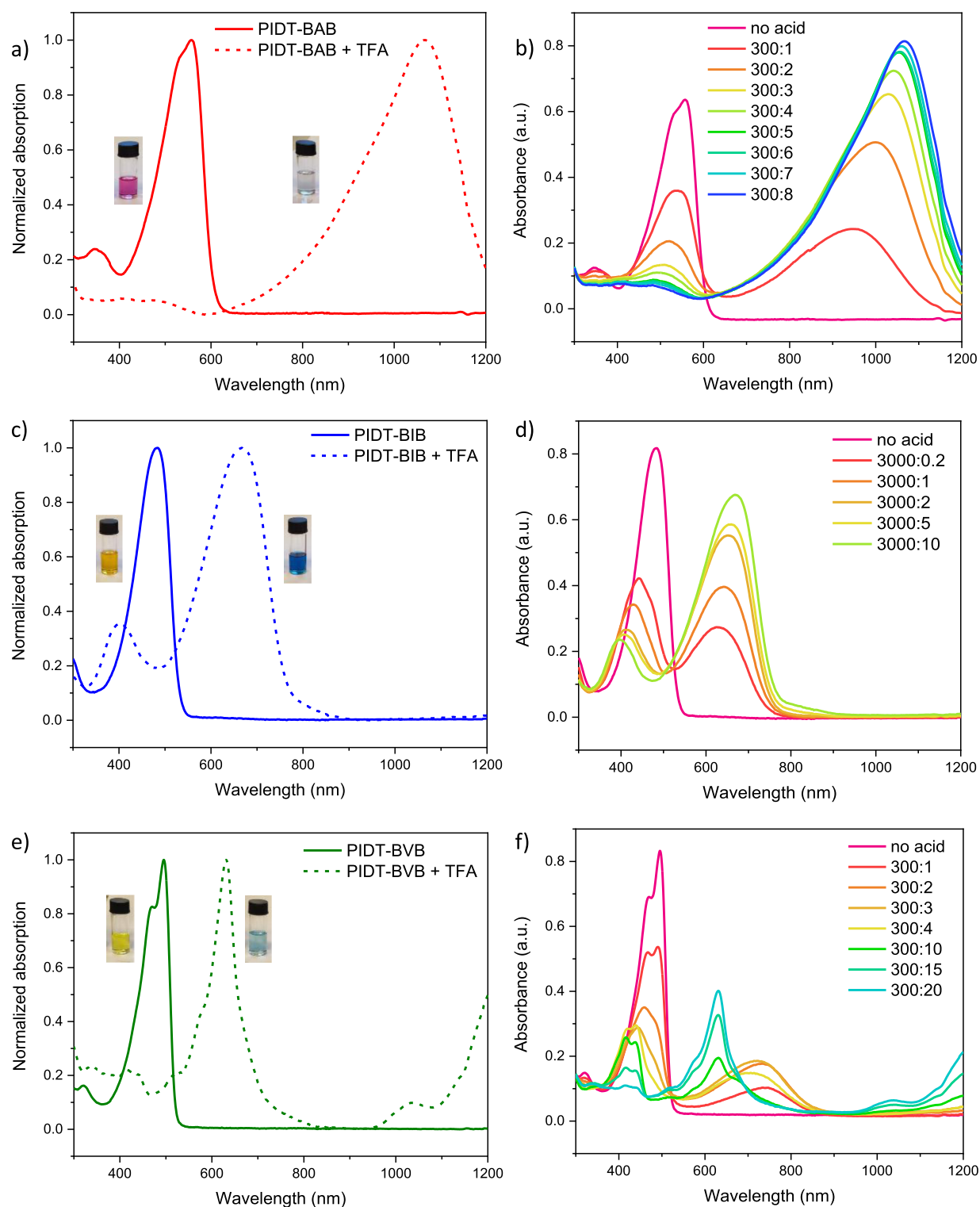


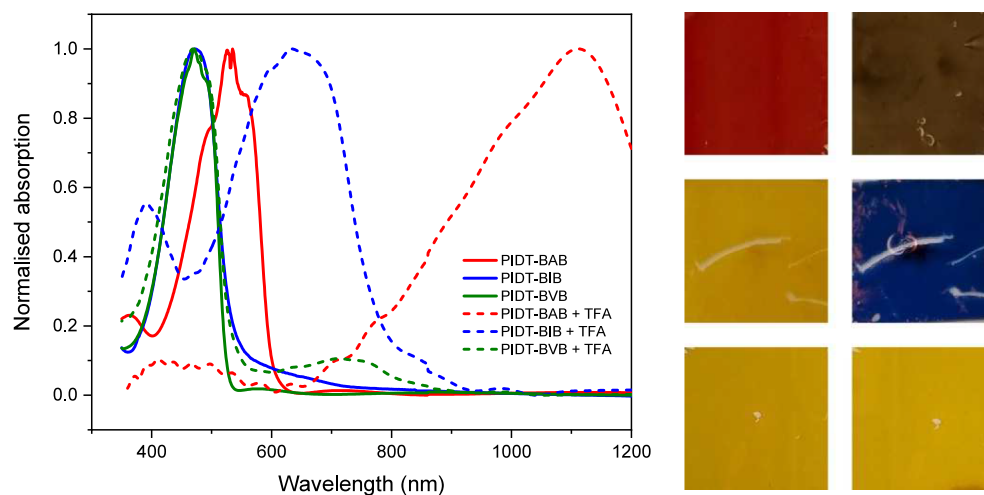
Figure 2. Left: UV-vis absorption spectra of $0.01 \text{ mg}\cdot\text{mL}^{-1}$ PIDT-BAB (a), PIDT-BIB (c), and PIDT-BVB (e) solutions in chloroform with and without the addition of trifluoroacetic acid (TFA). Photos of the solutions in UV-vis cuvettes are presented next to the corresponding spectra. Right: UV-vis absorption spectra of $0.01 \text{ mg}\cdot\text{mL}^{-1}$ PIDT-BAB (b), PIDT-BIB (d), and PIDT-BVB (f) solutions in chloroform with TFA at different volume ratios.

nm (change by 1.06 eV in energy) was observed for PIDT-BAB, turning the initially pink solution transparent upon the addition of TFA. PIDT-BIB and PIDT-BVB exhibited significantly smaller shifts of 183 nm (0.70 eV in energy) and 136 nm (0.54 eV in energy), respectively.

To further investigate the acidochromic behavior of the synthesized polymers, UV-vis spectra of the polymer solutions mixed with TFA in different volumetric ratios were collected (Figure 2). In the case of PIDT-BAB and PIDT-BIB, isosbestic points can be seen at 635 and 525 nm , respectively, marking the formation of new chemical species. With the gradual

Table 1. Absorption Maxima and Optical Band Gaps of the Synthesized Polymers in 0.01 mg·mL⁻¹ Solutions in Chloroform and in Thin-Film with and without the Addition of TFA

polymer	solution		solution + TFA		film		film + TFA	
	λ_{\max} [nm]	E_g^{opt} [eV]						
PIDT-BAB	557	2.09	1067	1.05	535	2.06	1111	0.92
PIDT-BIB	484	2.36	667	1.67	473	2.30	634	1.58
PIDT-BVB	495	2.40	631	1.88	471	2.35	469	2.32

**Figure 3.** Left: Normalized thin-film UV–vis absorption spectra of PIDT-BAB, PIDT-BIB, and PIDT-BVB with and without TFA. Right: Thin film of PIDT-BAB (top), PIDT-BIB (middle) and PIDT-BVB (bottom) before (left) and after (right) the addition of TFA.

increase in the TFA concentration, inverse shifts can be observed for the initial and newly formed absorption peaks. The former exhibits a hypsochromic shift, while the latter exhibits a bathochromic shift. As the isosbestic point marks a singular chemical transition and protonation has been reported as the mechanism for an acidochromic response of nitrogen-containing moieties, it can be concluded that protonation occurs at nitrogen atoms of azo and imine bonds. The protonation creates more electron-deficient regions in the polymer chain, which enhances the internal charge-transfer (ICT) effect from neighboring electron-rich IDT repeat units to the electron-deficient moieties, forming push–pull systems. As a result, the band gaps of the polymers are lowered, and the absorption spectra are red-shifted. As more nitrogen atoms in polymer chains are protonated, this change becomes more prominent, lowering the wavelengths of the absorption maxima of PIDT-BAB and PIDT-BIB in the presence of TFA.

The sensitivity of the synthesized polymers toward TFA varies largely. This can be observed clearly from the spectra in Figure 2, as PIDT-BIB exhibits a similar level of protonation to PIDT-BAB at a much smaller concentration of TFA, v/v ratios of 3000:0.2 and 300:1, respectively. This shows that the imine-containing PIDT-BIB is approximately 50 times more sensitive to TFA compared to its azo-containing equivalent. In contrast, a different behavior is observed in the case of PIDT-BVB, where no single isosbestic point can be determined. At the lowest TFA concentrations, an absorption peak around 740 nm is formed. With the further addition of TFA, it diminishes in favor of new absorption peaks at around 640 nm and broad peaks above 1000 nm. Given this complex pattern and the lack of protonation sites in the structure, it can be tentatively concluded that the process of chemical doping is responsible for the change in the spectral characteristics, in which radical cations (polarons) and bications (bipolarons) are formed in

the polymer backbone.³⁶ This is in line with previous studies, as both Lewis and Brønsted acids have previously been used as dopants in various conjugated polymer systems^{37–42} and TFA in particular has been applied as a dopant in triazole-containing conjugated polymers.⁴³

Fluorescent emission spectra of 0.01 mg·mL⁻¹ solutions of PIDT-BAB, PIDT-BIB, and PIDT-BVB in chloroform were collected before and after the addition of TFA. The recorded spectra are presented in Figure S3. Only the PIDT-BVB solution exhibited a significant emission with a maximum at 517 nm before the addition of TFA, which was quenched completely after the addition of TFA. PIDT-BIB emission was ~20 times lower than that of PIDT-BVB at its maximum at 553 nm, while PIDT-BAB exhibited virtually no emission at all.

Acidochromic properties of the polymers in thin films were investigated by UV–vis absorption spectrometry. The resulting spectra of the polymer films deposited on glass slides are shown in Figure 3 (left), together with pictures of the films before and after the addition of TFA (Figure 3 right). The spectra plotted in terms of energy are shown in Figure S2. The summary of the absorption properties is shown in Table 1. PIDT-BAB and PIDT-BIB exhibit similar behavior in the film and solution, with a significantly larger bathochromic shift in azo-containing PIDT-BAB compared to PIDT-BIB, almost twice as large in terms of energy (1.20 and 0.67 eV, respectively). This observation is important for the potential use of those polymers in sensor applications where the solid material is required. Notably, PIDT-BIB films were far more sensitive to TFA vapors compared to PIDT-BAB, switching color as soon as a TFA bottle was opened in its proximity. All of those observations form a strong argument for PIDT-BIB to be applied as an acid vapor sensor material. However, no meaningful change in the absorption spectrum was observed when PIDT-BVB was exposed to TFA, which is further proof

that its acidochromic properties in solution are not based on the same mechanism as for the other two polymers. To further verify the applicability of PIDT-BAB and PIDT-BIB as an acid sensor, the films and solutions in chloroform were exposed to a range of organic and inorganic acids: acetic acid, formic acid, hydrochloric acid, nitric acid, and sulfuric acid. Figures S15 and S16 show the color change in response to the exposure in thin films of PIDT-BAB and PIDT-BIB. Imine-containing PIDT-BIB was sensitive to all tested acids except for acetic acid, compared to PIDT-BAB, which did not respond to acetic, formic, or hydrochloric acid. Further conclusions were drawn from the exposure of polymer solutions in chloroform to the acids, as shown in Figures S17 and S18. PIDT-BAB solutions exhibited an interesting feature: significantly different absorption maxima depending on the acid used. This property could be used to identify the specific acid present, likely due to the influence of counterions. To confirm the relationship between the strength of the acid and the acidochromic response of the polymers, pK_a values of the polymers as well as acetic, formic, and trifluoroacetic acid were calculated using the B3LYP/6-31+G(d,p) level of theory. The results are presented in Table 2. The calculations present a credible reason for the difference

Table 2. Energetics of Protonation Reactions for Acetic, Formic, and TFA Acids, as well as Polymers^a

protonation reaction	ΔH in gas [kcal/mol]	pK_a in water	
		calcd	exptl
$\text{CH}_3\text{COO}^- + \text{H}^+ \rightarrow \text{CH}_3\text{COOH}$	-360.99	6.42	4.79 ⁴⁶
$\text{HCOO}^- + \text{H}^+ \rightarrow \text{HCOOH}$	-357.31	4.17	3.77 ⁴⁶
$\text{CF}_3\text{CO}_2^- + \text{H}^+ \rightarrow \text{CF}_3\text{CO}_2\text{H}$	-336.89	-2.49	0.23 ⁴⁶
$\text{PIDT-BAB} + \text{H}^+ \rightarrow \text{PIDT-BAB-H}^+$	-246.68	0.88	
$\text{PIDT-BIB} + \text{H}^+ \rightarrow \text{PIDT-BIB-H}^+$	-243.48	4.79	
$\text{PIDT-BVB} + \text{H}^+ \rightarrow \text{PIDT-BVB-H}^+$	-240.50	-5.84	
$\text{PIDT-BAB-H}^+ + \text{H}^+ \rightarrow \text{PIDT-BAB-2H}^+$	-182.76	-9.92	

^aThe enthalpy changes were calculated in the gas phase, while the pK_a values were determined in aqueous solution and considering the total Gibbs free energies of the protonated and deprotonated species. The calculations were performed using the B3LYP/6-31+G(d,p) level of theory. Solvent effects were accounted for using the SMD implicit solvation model. The gas-phase enthalpy and the Gibbs free energy of H^+ in water were taken from the literature, with values of -5.4 kcal/mol⁴⁴ and -265.9 kcal/mol,⁴⁵ respectively.

in the sensitivity of the three polymers. TFA, having a pK_a value lower than that of both PIDT-BAB and PIDT-BIB, can easily protonate both polymers, while formic acid can only protonate PIDT-BIB and not PIDT-BAB.

2.3. Electrochemical Properties. The oxidation and reduction potentials were measured for the synthesized polymers by using cyclic voltammetry in a three-electrode system. Polymer films were deposited on a Pt working electrode. The measurements were performed in 0.01 M tetrabutylammonium hexafluorophosphate solution in acetonitrile with a Pt wire counter electrode and a Ag wire pseudoreference electrode. The pseudoelectrode was calibrated with respect to the Fc/Fc^+ redox couple. The derived onset potentials for the electrochemical oxidation (E_{ox}) and reduction (E_{red}) were used for the determination of the highest occupied molecular orbital (HOMO) and lowest unoccupied molecular orbital (LUMO) energy levels using the equations $\text{HOMO} = -(E_{\text{ox}} + 5.13)$ eV and $\text{LUMO} = -(E_{\text{red}} + 5.13)$ eV. The cyclic voltammograms are provided in Figure

S12. The electrochemical band gaps of PIDT-BAB (2.26 eV) and PIDT-BVB (2.72 eV) correlate well with the optical band gaps, as presented in Table 1.

2.4. Sensor Cycling Performance. In order to evaluate the reversibility of the acidochromic transition, a cycling experiment was performed on the PIDT-BAB and PIDT-BIB films. The films were spin-coated on glass slides from 10 mg/mL-1 polymer solutions in chloroform at 3500 rpm. The films were repeatedly exposed to TFA vapor, flushed with nitrogen to remove TFA, and then exposed to triethylamine vapor. UV-vis spectra of the films were collected after a certain number of cycles. The recovery, determined as the ratio of absorbance at λ_{max} after cycling to the initial absorbance at λ_{max} , is plotted versus the number of cycles in Figure S4. While the PIDT-BAB film exhibited excellent recovery, the PIDT-BIB film showed a slow decrease in absorbance during cycling, reaching 86% of the initial value after 50 cycles.

Additionally, it was observed that the PIDT-BIB film required a significantly longer time to revert to the initial color at the end of the cycling experiment compared to the first cycle. In order to further investigate this phenomenon, another cycling experiment was conducted in a dedicated setup (Figure S5). A small tube was attached to the top of the UV-vis sample holder. Nitrogen flow was introduced into a glass junction with a valve switching between two outputs. One output was connected to an intermediary vial with TFA at the bottom and then to the tube on the sample holder; the other was connected directly to the tube. The single wavelength corresponding to the film absorption maximum was monitored via UV-vis spectroscopy over time. The film was constantly flushed with a nitrogen feed from the connected tube. The first cycle was started by manually turning the valve and directing the nitrogen flow through the vial containing TFA for 5 s. Then, the valve was switched back to pure nitrogen, and the film was left to recover. The same procedure was repeated for the next three cycles. The PIDT-BIB film cycling was monitored at 473 nm for 9 cycles (Figure S6 left). Times required to reach 95% of the absorbance at the plateau were then determined for each cycle. The results plotted in Figure S6 (right) show a gradual increase in recovery time. The absorbance after recovery decreased with the number of cycles as well. This could suggest that the deprotonation is not completed in a short time and some TFA remains within the polymer. The same setup was used for the PIDT-BAB film, but the change in absorbance observed when flushing the film with TFA-vapor and nitrogen was too small to be recorded, indicating lower sensitivity of PIDT-BAB toward TFA.

2.5. Acidochromic Mechanism from DFT Calculations.

Density functional theory (DFT) calculations were used to acquire a better understanding of the doping process of the synthesized polymers. At the B3LYP/6-311G(d,p) theory level, we simulated single repeating units of PIDT-BAB, PIDT-BIB, and PIDT-BVB, as well as their protonated and oxidized equivalents in a chloroform solution. HOMO and LUMO levels obtained from DFT are plotted in Figure S14. In the case of PIDT-BAB, protonation at a single and at both nitrogen atoms was considered. Optimized geometries show that protonation of both PIDT-BAB and PIDT-BIB increases planarity of the polymer chains (Figure 4). The angles between the IDT unit and first benzene ring decrease from 19.5° to 5.2° in PIDT-BAB and from 22.5° to 5.5° in PIDT-BIB. While in PIDT-BAB both benzene rings are coplanar in both neutral and protonated states, the imine bond in PIDT-BIB distorts

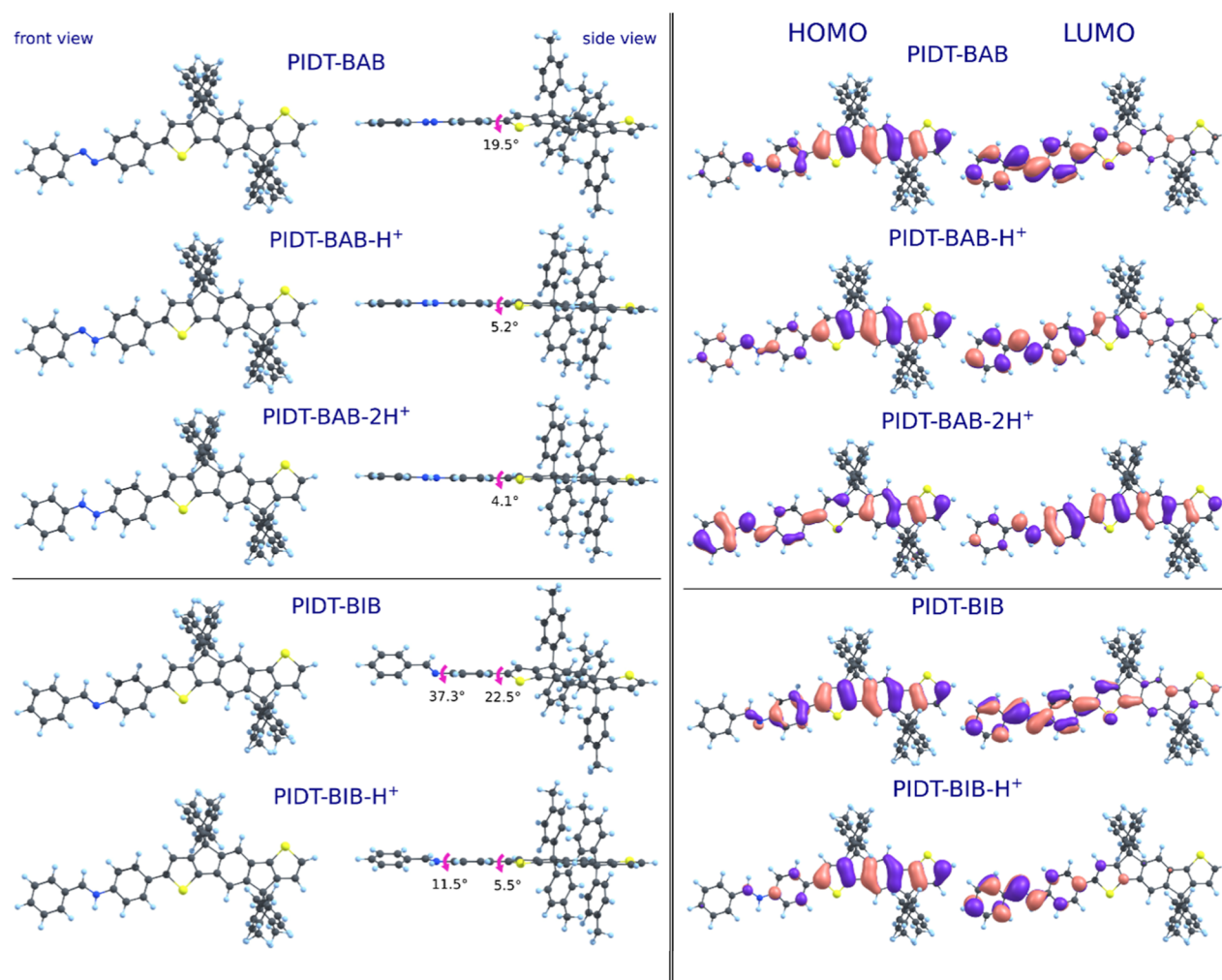


Figure 4. Left: DFT optimized geometry of the neutral, protonated ($-H^+$) and double protonated ($-2H^+$) PIDT-BAB, as well as neutral and protonated ($-H^+$) PIDT-BIB in chloroform solution. Front view on the left, side view on the right side. Right: HOMO (left) and LUMO (right) density plots (isovalue = 0.05) of the neutral, protonated, and double protonated PIDT-BAB, as well as neutral and protonated PIDT-BIB in chloroform solution.

this planarity by 37.3° in the neutral state. This angle decreases at protonation to 11.5° ; however, it results in a less planar structure than in PIDT-BAB. Double protonation further planarizes the PIDT-BAB core, reducing the dihedral angle to 4.1° . Because more planar structures can lead to more extensive conjugation lengths, this provides an explanation for the unusually large bathochromic shift of the absorption spectra of PIDT-BAB upon protonation, especially compared to the corresponding PIDT-BIB and PIDT-BVB spectra (see Figure 2). HOMO–LUMO density plots (Figure 4) reveal another difference between PIDT-BAB and PIDT-BIB. Whereas protonation promotes electronic delocalization in PIDT-BAB, it results in increased localization in PIDT-BIB.

Time-dependent DFT was used to simulate UV–vis–NIR spectra of neutral, protonated, and oxidized PIDT-BAB and PIDT-BIB in chloroform solution (Figure 5). The simulated spectra of protonated PIDT-BAB and PIDT-BIB exhibit a good correlation with experimental results. A closer analysis of the UV–vis absorption spectrum of protonated PIDT-BAB (Figure 2) suggests that protonation may occur at both nitrogen atoms. The asymmetric profile of the absorption peak at ~ 800 – 1200 nm with a shoulder peak at lower wavelengths and bathochromic shift of the peak at higher concentrations of

TFA correspond well to the result of DFT calculations (Figure 5). The simulated oxidized absorption spectra of both PIDT-BAB and PIDT-BIB exhibit a strong absorption maximum at ~ 1100 nm. However, the absence of absorption peaks at ~ 1100 nm in both the experimental and simulated UV–vis spectra of the protonated species confirms that the interaction between the polymers and TFA is not a redox reaction. To provide further experimental proof, a thin film of PIDT-BAB was deposited on an ITO-coated glass substrate and oxidized by applying a positive potential. The resulting spectrum, as displayed in Figure S13, reveals that the oxidized PIDT-BAB film shows strong absorption in the NIR region, a feature not observed in the TFA-treated films. Based on those results, it can be concluded that the acidochromic response of PIDT-BAB occurs as a result of protonation.

In the case of PIDT-BVB, as there is no N atom as an obvious protonation site, the acid doping mechanism was investigated by simulating protonation at various sites of the molecule (Figure 6). In each case, the initial step was considered to be the electrophilic addition of a proton to a double bond.⁴⁷ This breaks a double bond in the aromatic system, resulting in an sp^3 carbon and a carbocation on the atoms which formed the broken bond. Five protonation sites

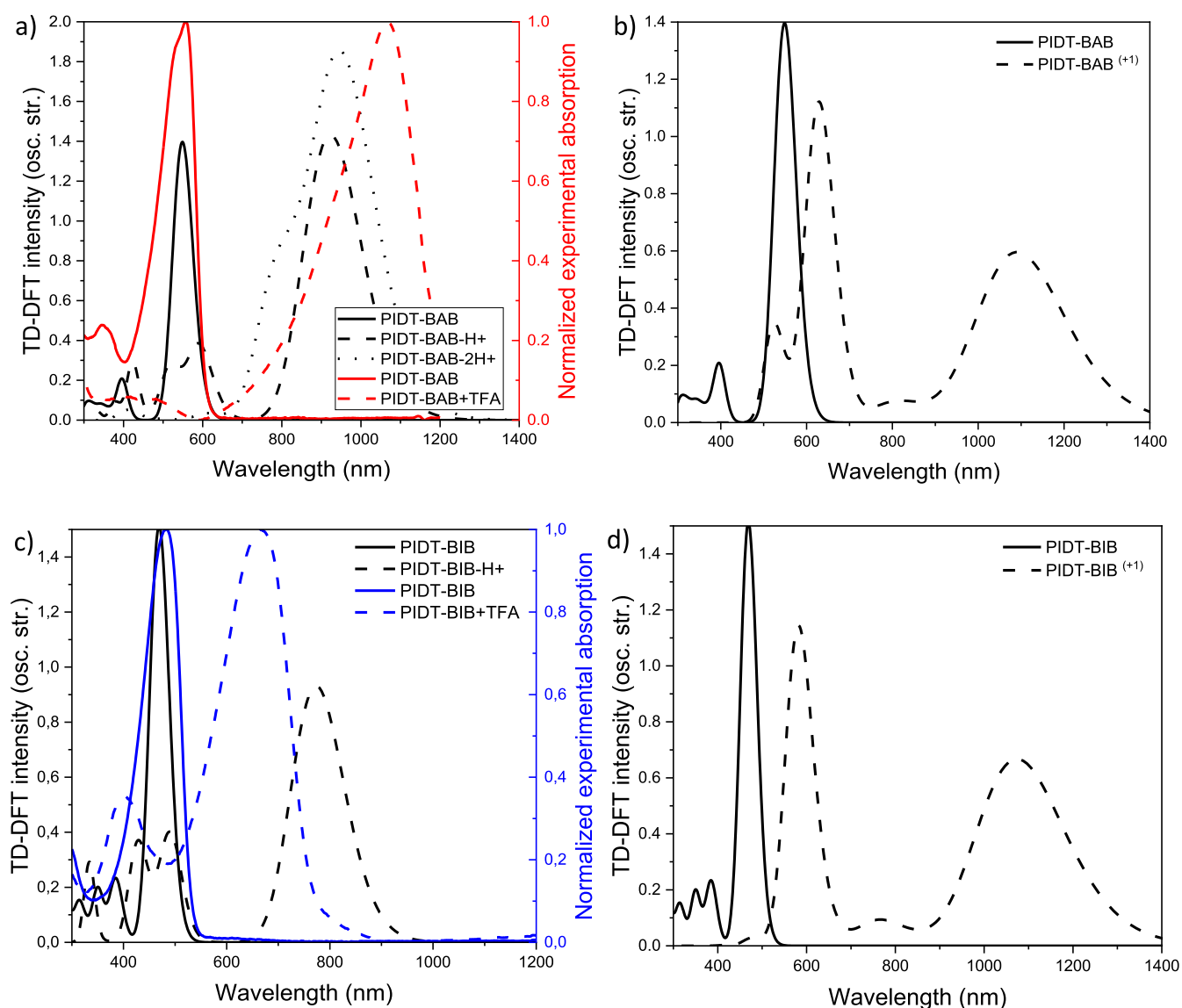


Figure 5. (a) Experimental (red) and TD-DFT (black) absorption spectra of neutral (solid), protonated (dashed), and double protonated (dotted) species of PIDT-BAB in chloroform solution. (b) TD-DFT electronic spectra of neutral (solid) and oxidized (dashed) species of PIDT-BAB in chloroform solution. (c) Experimental (blue) and TD-DFT (black) electronic spectra of neutral (solid) and protonated (dashed) species of PIDT-BIB in chloroform solution. (d) TD-DFT electronic spectra of neutral (solid) and oxidized (dashed) species of PIDT-BIB in chloroform solution. All TD-DFT electronic excitations convoluted with a Gaussian function of 0.25 eV of full width at half-maximum.

are taken into consideration, as shown in Figure 6a. Calculated values of the protonation enthalpy changes (ΔH) do not vary significantly, indicating that protonation could occur at any one of these sites. On the other hand, the band gaps of the protonated conformers differ largely depending on the protonation site. TD-DFT UV–vis absorption spectra shown in Figure 6c exhibit absorption peaks at many different wavelengths, which correlates with the multitude of spectroscopic features visible in the experimental spectrum of PIDT-BVB solution in chloroform with the addition of TFA (Figure 2e,f). Optimized geometries of the protonated conformers visualize the large changes in the conformation occurring at the protonation of PIDT-BVB. The resulting sp^3 carbon introduces a bending point in the structure, which requires large segments of the polymer to move. Therefore, protonation occurs easily in solution, but not in the film, as the polymer chains have limited mobility in the solid state to bend and rotate. An experimental UV–vis–NIR absorption spectrum of the

oxidized PIDT-BVB deposited on an ITO-coated glass substrate (Figure S13) exhibits features similar to those of the protonated PIDT-BVB solution in chloroform, showing that polaron formation occurs once the polymer chain is protonated. These discussed findings lead to the conclusion that acid doping is the mechanism behind the acidochromic response of PIDT-BVB.

3. CONCLUSIONS

In this work, three IDT-based conjugated polymers containing azo, imine, and vinyl bonds (PIDT-BAB, PIDT-BIB, and PIDT-BVB, respectively) have been synthesized by Stille coupling. Their acidochromic behaviors were investigated using UV–vis absorption and emission spectroscopy, cyclic voltammetry, and repeated exposure to TFA and DFT calculations. It has been found that all three polymers exhibit an acidochromic response to TFA in solution. The sensitivity of polymers differed by orders of magnitude, with PIDT-BIB

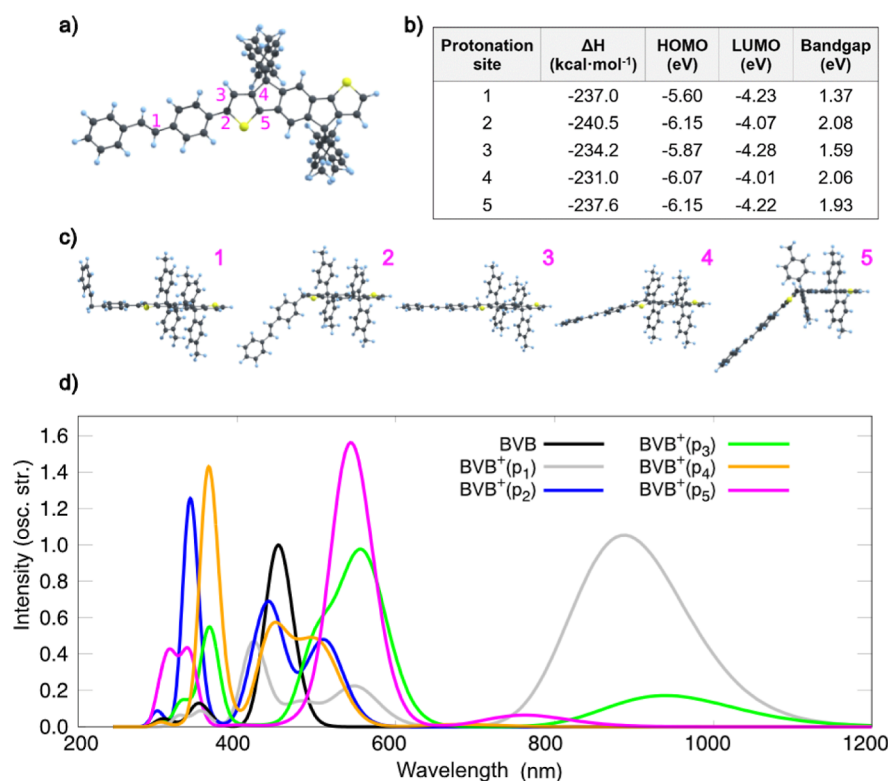


Figure 6. (a) BVB repeating unit with protonation sites labeled. (b) Protonation enthalpy changes (ΔH), HOMO, LUMO and band gaps for the BVB⁺ protonated at the corresponding protonation sites. Enthalpy changes calculated in the gas phase. HOMO, LUMO, and band gaps calculated in chloroform. (c) Optimized geometries of BVB⁺ protonated at the corresponding protonation sites. (d) TD-DFT absorption spectra of BVB⁺ conformers protonated at the corresponding protonation sites. TD-DFT electronic excitations convoluted with a Gaussian function of 0.25 eV of full width at half-maximum.

being the most sensitive and PIDT-BVB the least sensitive. PIDT-BAB and PIDT-BIB behaved similarly in thin film as in solution, while PIDT-BVB showed no response to acid in the solid state. Notable is the large bathochromic shift of 510 nm in the UV–vis absorption of PIDT-BAB after protonation, unprecedented in the literature on acidochromic materials. The superior band gap narrowing, enabled by the orbital delocalization of multiple monomer units, could be achieved thanks to the long-chain structure, a distinctive advantage of conjugated polymers over small molecules. The pink to transparent change in solution (or red to gray in the thin film) is particularly interesting for use in display sensors. Cyclic TFA-exposure experiments on PIDT-BAB and PIDT-BIB films revealed the differences in sensitivity and stability. The PIDT-BAB film was less sensitive to acid vapors, but the acidochromic switching was reversible without loss in performance after 50 cycles. In contrast, highly sensitive PIDT-BIB showed a gradual retention of TFA, with an 85% recovery after 50 cycles. An extremely fast and highly sensitive response of PIDT-BIB to vapors of various organic and inorganic acids makes it an ideal material for acid sensors. DFT calculations showed an increase in the planarity of the PIDT-BAB and PIDT-BIB backbones after protonation. This effect was significantly stronger in PIDT-BAB, resulting in the aforementioned large bathochromic shift in UV–vis absorption. TD-DFT simulated UV–vis–NIR absorption spectra of protonated and oxidized films provided additional confirmation of the doping mechanism in the investigated polymers. It was found that the mechanism of the acidochromic response was the same for azo- and imine-containing polymers, which

occurred by protonation at nitrogen atoms. In contrast, vinyl-containing PIDT-BVB underwent acid doping in a chloroform solution, resulting in the formation of polarons in the conjugated polymer and the change of absorption characteristics. Those insights offer a more systematic comparison of the three moieties, which can be used as a guideline for the design of acidochromic sensors.

4. EXPERIMENTAL SECTION

4.1. Materials. 4-Bromoaniline, 4-bromobenzaldehyde, tris(dibenzylideneacetone)dipalladium(0) (Pd₂(dba)₃), tri(*o*-tolyl)-phosphine, copper(I) bromide, pyridine, and 4,4′-dibromo-*trans*-stilbene were purchased from Sigma-Aldrich. Toluene, acetone, diethyl ether, and chloroform were purchased from VWR. (4,4,9,9-Tetrakis(4-octylphenyl)-4,9-dihydro-*s*-indaceno[1,2-*b*:5,6-*b*′]-dithiophene-2,7-diyl)bis(trimethylstannane) (IDT-Sn) was purchased from Solarmer Materials.

4.2. Characterization. The synthesized products were analyzed with ¹H NMR spectroscopy by using a Bruker 600 MHz NMR spectrometer. Molecular weights of synthesized polymers were determined by gel permeation chromatography (GPC) on an Agilent PL-GPC 220 integrated high-temperature GPC/SEC system equipped with refractive index and viscometer detectors and three sequential PLgel 10 μm MIXED-B LS 300 mm × 7.5 mm columns, using 1,2,4-trichlorobenzene as an eluent at 150 °C. UV–vis absorption spectra were collected on a PerkinElmer Lambda 1050 UV/vis/NIR spectrometer at room temperature. FTIR spectra were recorded on a PerkinElmer Spectrum 3 FT-IR/NIR/FIR spectrometer in the ATR mode. Thermal gravimetric analysis (TGA) was conducted on a Mettler Toledo TGA/DSC 3+ STAR System instrument.

4.3. Synthesis. **4.3.1. Synthesis of Monomers.** 4-Bromoaniline (3.00 g, 17.44 mmol) (1) was reacted with 4-bromobenzaldehyde (3.23 g, 17.44 mmol) in 50 mL of ethanol at 90 °C overnight. The reaction mixture was then placed in a refrigerator to cool down. Precipitated white crystals were collected via filtration. The crude product was recrystallized from methanol/ethanol (1:1 vol.) and dried in a vacuum oven. The yield was 2.55 g (43%) of *N*,1-bis(4-bromophenyl)methanimine (4). ¹H NMR (CDCl₃, 600 MHz): δ (ppm) 8.40 (s, 1H), 7.78 (d, 2H), 7.64 (d, 2H), 7.53 (d, 2H), 7.11 (d, 2H). Full ¹H NMR spectrum is in Figure S8. FTIR spectrum is shown in Figure S19.

4-Bromoaniline (10.00 g, 58.13 mmol), CuBr (0.25 g, 1.74 mmol), and pyridine (0.41 g, 5.23 mmol) were reacted in 60 mL of toluene at room temperature for 4 days. The reaction mixture was then dried on a rotary evaporator. The crude product was filtered on a sintering glass and washed with methanol. The solid was dissolved in 20 mL of boiling toluene and placed in the fridge. The recrystallized product was washed with methanol and dried to obtain 5.29 g (54% yield) of 1,2-bis(4-bromophenyl)diazene (2). ¹H NMR (CDCl₃, 600 MHz): δ (ppm) 7.73 (d, 4H), 7.58 (d, 4H). The full ¹H NMR spectrum is in Figure S7. The FTIR spectrum is shown in Figure S19.

4.3.2. Synthesis of PIDT-BAB (3). 1,2-Bis(4-bromophenyl)diazene (2) (100.0 mg, 0.294 mmol), IDT-Sn (396.6 mg, 0.294 mmol), Pd₂(dba)₃ (5.4 mg, 0.006 mmol), and tri(*o*-tolyl)phosphine (7.2 mg, 0.024 mmol) were placed in a double-necked flask, connected to a condenser, and flushed with nitrogen. Then, 10 mL of dry and degassed toluene was added. The reaction mixture was stirred at 100 °C for 35 min. Then, the reaction mixture was cooled down, concentrated in vacuo and precipitated in methanol. The crude polymer was purified by Soxhlet extraction with acetone, diethyl ether, and chloroform. The solvent was removed from the chloroform fraction in a rotary evaporator. The concentrated polymer was precipitated in methanol, filtered, and dried in a vacuum oven at 40 °C overnight. The product was collected as a red solid with golden shine (340 mg, 96% yield). Number-average molecular weight (M_n): 53.8 kg·mol⁻¹, weight-average molecular weight (M_w): 120.9 kg·mol⁻¹, and polydispersity index (PDI): 2.245. The GPC spectrum is shown in Figure S9. The FTIR spectrum is shown in Figure S20.

4.3.3. Synthesis of PIDT-BIB (5). *N*,1-Bis(4-bromophenyl)methanimine (100.0 mg, 0.295 mmol) (4), IDT-Sn (396.8 mg, 0.295 mmol), Pd₂(dba)₃ (5.4 mg, 0.006 mmol), and tri(*o*-tolyl)phosphine (7.2 mg, 0.012 mmol) were placed in a double-necked flask, connected to a condenser, and flushed with nitrogen. Then, 10 mL of dry and degassed toluene was added. The reaction mixture was stirred at 100 °C for 150 min. Then, the reaction mixture was cooled down, concentrated in vacuo, and precipitated in methanol. The crude polymer was purified by Soxhlet extraction with acetone, diethyl ether, and chloroform. The solvent was removed from the chloroform fraction in a rotary evaporator. The concentrated polymer was precipitated in methanol, filtered, and dried in a vacuum oven at 40 °C overnight. The product was collected as an orange solid (313 mg, 86% yield). Number-average molecular weight (M_n): 18.0 kg·mol⁻¹, weight-average molecular weight (M_w): 37.1 kg·mol⁻¹, and polydispersity index (PDI): 2.064. GPC spectrum is shown in Figure S10. The FTIR spectrum is shown in Figure S20. The TGA thermogram is shown in Figure S21.

4.3.4. Synthesis of PIDT-BVB (7). 4,4'-Dibromo-*trans*-stilbene (50.0 mg, 0.148 mmol) (6), IDT-Sn (199.0 mg, 0.148 mmol), Pd₂(dba)₃ (2.71 mg, 0.003 mmol), and tri(*o*-tolyl)phosphine (3.6 mg, 0.012 mmol) were placed in a double-necked flask, connected to a condenser, and flushed with nitrogen. Then, 10 mL of dry and degassed toluene was added. The reaction mixture was stirred at 100 °C for 70 min. Then, the reaction mixture was cooled down, concentrated in vacuo, and precipitated in methanol. The crude polymer was purified by Soxhlet extraction with acetone, diethyl ether, and chloroform. The solvent was removed from the chloroform fraction in a rotary evaporator. The concentrated polymer was precipitated in methanol, filtered, and dried in a vacuum oven at 40 °C overnight. The product was collected as an orange solid (128 mg, 72% yield). Number-average molecular weight (M_n): 44.6 kg·mol⁻¹,

weight-average molecular weight (M_w): 126.2 kg·mol⁻¹, and polydispersity index (PDI): 2.832. GPC spectrum is shown in Figure S11. The FTIR spectrum is shown in Figure S20. The TGA thermogram is shown in Figure S22.

4.4. Theoretical Modeling. The electronic structure of PIDT-BAB, PIDT-BIB, and PIDT-BVB was studied utilizing the density functional theory (DFT) and its time-dependent version (TD-DFT). At the B3LYP⁴⁸/6-311+G(d,p)⁴⁹ theory level, we performed the geometry optimization of monomeric models of the polymers and calculated the thermal corrections to the Gibbs free energy. In order to explore the acidochromic effects in the electronic structure of the compounds, we calculated the electronic properties of the monocationic and dicationic species of PIDT-BAB and the monocationic species of PIDT-BIB by protonating the azobenzene-like nitrogen. Besides, we also analyzed the effects of the electronic oxidation of all of the systems, calculating the open-shell electronic structure of the monoanionic/half-spin species of the compounds, by considering geometry relaxation effects. The energy levels of the systems were calculated by considering the full Gibbs free energy of the neutral and charged species within the diabatic approximation, where the reorganization energy of the charged species is fully accounted. The first 10 electronic transitions of each compound were calculated using TD-DFT and the electronic absorption spectra were convoluted using Gaussian functions. All calculations were realized considering environment effects using the implicit SMD model⁵⁰ at the dielectric constant of chloroform ($\epsilon = 4.71$). The alkyl side chains of IDT were substituted with methyl groups to simplify the calculations. The calculations were carried out using a Gaussian 16 program (Rev C.01).⁵¹

■ ASSOCIATED CONTENT

Supporting Information

The Supporting Information is available free of charge at <https://pubs.acs.org/doi/10.1021/acs.macromol.4c02700>.

DFT electronic properties, Tauc plots, UV-vis absorption spectra, UV-vis emission spectra, recovery of absorption, acidochromic cycling experiment, H NMR, cyclic voltammograms, GPC, TGA, DFT, PIDT-BAB and PIDT-BIB thin films, and FTIR (PDF)

■ AUTHOR INFORMATION

Corresponding Authors

Moyses Araujo – Department of Engineering and Physics, Karlstad University, 651 88 Karlstad, Sweden; Materials Theory Division, Department of Physics and Astronomy, Uppsala University, 751 20 Uppsala, Sweden; Email: moyses.araujo@kau.se

Ergang Wang – Department of Chemistry and Chemical Engineering, Chalmers University of Technology, 412 96 Göteborg, Sweden; orcid.org/0000-0002-4942-3771; Email: ergang@chalmers.se

Authors

Krzysztof Kotewicz – Department of Chemistry and Chemical Engineering, Chalmers University of Technology, 412 96 Göteborg, Sweden

Leandro R. Franco – Department of Engineering and Physics, Karlstad University, 651 88 Karlstad, Sweden; orcid.org/0000-0002-8692-3396

Complete contact information is available at: <https://pubs.acs.org/doi/10.1021/acs.macromol.4c02700>

Notes

The authors declare no competing financial interest.

ACKNOWLEDGMENTS

We thank the Swedish Research Council (2021-04778, 2019-02345, and 2018-07072), the Swedish Energy Agency (P2021-00032 and 50779-1), STINT, Bertil & Britt Svenssons stiftelse för belysningsteknik (2021 höst-14 and 2022 höst-31), the Knut and Alice Wallenberg Foundation (2022.0192, WISE-AP01-D02), and the Wallenberg Initiative Materials Science for Sustainability, WISE. for financial support. We acknowledge the Swedish Research Council (Grant no. 2020-05223), the Swedish Energy Agency (Grant no. 45420-1), and the STandUP for energy collaboration for financial support. The computations were enabled by resources provided by the National Academic Infrastructure for Supercomputing in Sweden (NAISS) and the Swedish National Infrastructure for Computing (SNIC) at the National Supercomputer Centre (NSC) at Linköping University, partially funded by the Swedish Research Council through Grant Agreement nos. 2022-06725 and 2018-05973.

REFERENCES

- (1) Su, X.; Wang, Y.; Fang, X.; Zhang, Y.-M.; Zhang, T.; Li, M.; Liu, Y.; Lin, T.; Zhang, S. X.-A. A High Contrast Tri-state Fluorescent Switch: Properties and Applications. *Chem.—Asian J.* **2016**, *11* (22), 3205–3212.
- (2) Lin, T.; Su, X.; Wang, K.; Li, M.; Guo, H.; Liu, L.; Zou, B.; Zhang, Y.-M.; Liu, Y.; Zhang, S. X.-A. An AIE fluorescent switch with multi-stimuli responsive properties and applications for quantitatively detecting pH value, sulfite anion and hydrostatic pressure. *Mater. Chem. Front.* **2019**, *3* (6), 1052–1061.
- (3) Su, X.; Ji, Y.; Pan, W.; Chen, S.; Zhang, Y.-M.; Lin, T.; Liu, L.; Li, M.; Liu, Y.; Zhang, S. X.-A. Pyrene spiropyran dyad: solvato-, acido- and mechanofluorochromic properties and its application in acid sensing and reversible fluorescent display. *J. Mater. Chem. C* **2018**, *6* (26), 6940–6948.
- (4) Qin, T.; Han, J.; Geng, Y.; Ju, L.; Sheng, L.; Zhang, S. X.-A. A Multiaddressable Dyad with Switchable Cyan/Magenta/Yellow Colors for Full-Color Rewritable Paper. *Chem.—Eur. J.* **2018**, *24* (48), 12539–12545.
- (5) Xi, G.; Sheng, L.; Du, J.; Zhang, J.; Li, M.; Wang, H.; Ma, Y.; Zhang, S. X.-A. Water assisted biomimetic synergistic process and its application in water-jet rewritable paper. *Nat. Commun.* **2018**, *9* (1), 4819.
- (6) Razavi, B.; Roghani-Mamaqani, H.; Salami-Kalajahi, M. Rewritable acidochromic papers based on oxazolidine for anti-counterfeiting and photosensing of polarity and pH of aqueous media. *Sci. Rep.* **2022**, *12* (1), 9412.
- (7) Bhuin, S.; Samanta, P. K.; Chakravarty, M. Efficient and reversible acidofluorochromic features on a solid platform for reusable security writing: A structure-property relationship study on anthracenyl π -conjugates. *Dyes Pigm.* **2022**, *197*, 109944.
- (8) Cesaretti, A.; Bonaccorso, C.; Carboni, V.; Giubila, M. S.; Fortuna, C. G.; Elisei, F.; Spalletti, A. Four styryl phenanthroline derivatives as excellent acidochromic probes. *Dyes Pigm.* **2019**, *162*, 440–450.
- (9) Genovese, M. E.; Abraham, S.; Caputo, G.; Nanni, G.; Kumaran, S. K.; Montemagno, C. D.; Athanassiou, A.; Fragouli, D. Photochromic Paper Indicators for Acidic Food Spoilage Detection. *ACS Omega* **2018**, *3* (10), 13484–13493.
- (10) Zhang, L.; Naumov, P. Light- and Humidity-Induced Motion of an Acidochromic Film. *Angew. Chem., Int. Ed.* **2015**, *54* (30), 8642–8647.
- (11) Wang, Y.; Chen, Q.; Liu, Z.; Yu, F.; Su, W.; Cai, Z.; Guan, W.; Li, Y.; Sheng, L.; Qi, Z.; et al. Acidochromic organic photovoltaic integrated device. *Chem. Eng. J.* **2023**, *452*, 139479.
- (12) Zhang, J.; Chen, J.; Xu, B.; Wang, L.; Ma, S.; Dong, Y.; Li, B.; Ye, L.; Tian, W. Remarkable fluorescence change based on the protonation–deprotonation control in organic crystals. *Chem. Commun.* **2013**, *49* (37), 3878–3880.
- (13) Hariharan, P. S.; Mothi, E. M.; Moon, D.; Anthony, S. P. Halochromic Isoquinoline with Mechanochromic Triphenylamine: Smart Fluorescent Material for Rewritable and Self-Erasable Fluorescent Platform. *ACS Appl. Mater. Interfaces* **2016**, *8* (48), 33034–33042.
- (14) Black, H. T.; Pelse, I.; Wolfe, R. M. W.; Reynolds, J. R. Halochromism and protonation-induced assembly of a benzo[g]-indolo[2,3-b]quinoxaline derivative. *Chem. Commun.* **2016**, *52* (87), 12877–12880.
- (15) Li, M.; Yuan, Y.; Chen, Y. Acid-Induced Multicolor Fluorescence of Pyridazine Derivative. *ACS Appl. Mater. Interfaces* **2018**, *10* (1), 1237–1243.
- (16) Zhang, Y.; Huang, J.; Kong, L.; Tian, Y.; Yang, J. Two novel AIEE-active imidazole/ α -cyanostilbene derivatives: photophysical properties, reversible fluorescence switching, and detection of explosives. *CrystEngComm* **2018**, *20* (9), 1237–1244.
- (17) Yahya, M.; Metin, R.; Aydiner, B.; Seferoğlu, N.; Seferoğlu, Z. The syntheses, photophysical properties and pH-sensitive studies of heterocyclic azo dyes bearing coumarin–thiophene–thiazole. *Anal. Sci.* **2023**, *39* (6), 829–842.
- (18) Li, M.; Niu, Y.; Lu, H.-Y.; Chen, C.-F. Tetrahydro[5]helicene-based dye with remarkable and reversible acid/base stimulated fluorescence switching properties in solution and solid state. *Dyes Pigm.* **2015**, *120*, 184–189.
- (19) Sachdeva, T.; Gupta, S.; Milton, D. M. Smart Organic Materials with Acidochromic Properties. *Curr. Org. Chem.* **2020**, *24* (17), 1976–1998.
- (20) Wu, X.; Wang, W.; Li, B.; Hou, Y.; Niu, H.; Zhang, Y.; Wang, S.; Bai, X. Synthesis and electrochromic, acidochromic properties of Schiff bases containing triphenylamine and thiophene units. *Spectrochim. Acta, Part A* **2015**, *140*, 398–406.
- (21) Ndwandwe, B. K.; Malinga, S. P.; Kayitesi, E.; Dlamini, B. C. Recent developments in the application of natural pigments as pH-sensitive food freshness indicators in biopolymer-based smart packaging: challenges and opportunities. *Int. J. Food Sci. Technol.* **2024**, *59* (4), 2148–2161.
- (22) Palani, P.; Karpagam, S. Conjugated polymers – a versatile platform for various photophysical, electrochemical and biomedical applications: a comprehensive review. *New J. Chem.* **2021**, *45* (41), 19182–19209.
- (23) Pankow, R. M.; Thompson, B. C. The development of conjugated polymers as the cornerstone of organic electronics. *Polymer* **2020**, *207*, 122874.
- (24) Guo, X.; Baumgarten, M.; Müllen, K. Designing π -conjugated polymers for organic electronics. *Prog. Polym. Sci.* **2013**, *38* (12), 1832–1908.
- (25) Genee, Z.; Xia, Z.; Yang, G.; Mammo, W.; Wang, E. Recent Advances in the Synthesis of Conjugated Polymers for Supercapacitors. *Adv. Mater. Technol.* **2024**, *9* (9), 2300167.
- (26) Ma, L.; Cai, J.; Zhao, P.; Niu, H.; Wang, C.; Bai, X.; Wang, W. In situ preparation of composite from conjugated polyschiff bases and multiwalled carbon nanotube: Synthesis, electrochromic, acidochromic properties. *Mater. Chem. Phys.* **2012**, *133* (1), 333–339.
- (27) Bathula, C.; Henry, O.; Kumar K, A.; K, S.; Jana, A.; Rabani, I.; Choi, J.-H.; Jeon, J.-H.; Kim, H.-S. Facile synthesis of an indacenodithiophene-based conjugated polymer for acid vapor sensing. *Dyes Pigm.* **2021**, *184*, 108847.
- (28) Genovese, M. E.; Colusso, E.; Colombo, M.; Martucci, A.; Athanassiou, A.; Fragouli, D. Acidochromic fibrous polymer composites for rapid gas detection. *J. Mater. Chem. A* **2017**, *5* (1), 339–348.
- (29) Genovese, M. E.; Athanassiou, A.; Fragouli, D. Photoactivated acidochromic elastomeric films for on demand acidic vapor sensing. *J. Mater. Chem. A* **2015**, *3* (44), 22441–22447.
- (30) Benkhaya, S.; M'Rabet, S.; El Harfi, A. Classifications, properties, recent synthesis and applications of azo dyes. *Heliyon* **2020**, *6* (1), No. e03271.

- (31) Sperner, M.; Tober, N.; Detert, H. Triazolotriazines with Azobenzene Arms - Acidochromic Dyes and Discotic Liquid Crystals. *Eur. J. Org. Chem.* **2019**, *2019* (29), 4688–4693.
- (32) Wang, J.; Meng, Q.; Yang, Y.; Zhong, S.; Zhang, R.; Fang, Y.; Gao, Y.; Cui, X. Schiff Base Aggregation-Induced Emission Luminogens for Sensing Applications: A Review. *ACS Sens.* **2022**, *7* (9), 2521–2536.
- (33) Li, Y.; Gu, M.; Pan, Z.; Zhang, B.; Yang, X.; Gu, J.; Chen, Y. Indacenodithiophene a promising building block for high performance polymer solar cells. *J. Mater. Chem. A* **2017**, *5* (22), 10798–10814.
- (34) Müllen, K.; Pisula, W. Donor–Acceptor Polymers. *J. Am. Chem. Soc.* **2015**, *137* (30), 9503–9505.
- (35) Makula, P.; Pacia, M.; Macyk, W. How To Correctly Determine the Band Gap Energy of Modified Semiconductor Photocatalysts Based on UV–Vis Spectra. *J. Phys. Chem. Lett.* **2018**, *9* (23), 6814–6817.
- (36) Zozoulenko, I.; Singh, A.; Singh, S. K.; Gueskine, V.; Crispin, X.; Berggren, M. Polarons, Bipolarons, And Absorption Spectroscopy of PEDOT. *ACS Appl. Polym. Mater.* **2019**, *1* (1), 83–94.
- (37) Yurash, B.; Cao, D. X.; Brus, V. V.; Leifert, D.; Wang, M.; Dixon, A.; Seifrid, M.; Mansour, A. E.; Lungwitz, D.; Liu, T.; et al. Towards understanding the doping mechanism of organic semiconductors by Lewis acids. *Nat. Mater.* **2019**, *18* (12), 1327–1334.
- (38) Han, C. C.; Elsenbaumer, R. L. Protonic acids: Generally applicable dopants for conducting polymers. *Synth. Met.* **1989**, *30* (1), 123–131.
- (39) McQuillan, B.; Street, G. B.; Clarke, T. C. The reaction of hf with polyacetylene. *J. Electron. Mater.* **1982**, *11* (3), 471–490.
- (40) Suh, E. H.; Oh, J. G.; Jung, J.; Noh, S. H.; Lee, T. S.; Jang, J. Brønsted Acid Doping of P3HT with Largely Soluble Tris-(pentafluorophenyl)borane for Highly Conductive and Stable Organic Thermoelectrics Via One-Step Solution Mixing. *Adv. Energy Mater.* **2020**, *10* (47), 2002521.
- (41) Poverenov, E.; Zamoshchik, N.; Patra, A.; Ridelman, Y.; Bendikov, M. Unusual Doping of Donor–Acceptor-Type Conjugated Polymers Using Lewis Acids. *J. Am. Chem. Soc.* **2014**, *136* (13), 5138–5149.
- (42) Hofmann, A. I.; Kroon, R.; Yu, L.; Müller, C. Highly stable doping of a polar polythiophene through co-processing with sulfonic acids and bistriflimide. *J. Mater. Chem. C* **2018**, *6* (26), 6905–6910.
- (43) Martwiset, S.; Woudenberg, R. C.; Granados-Focil, S.; Yavuzcetin, O.; Tuominen, M. T.; Coughlin, E. B. Intrinsically conducting polymers and copolymers containing triazole moieties. *Solid State Ionics* **2007**, *178* (23), 1398–1403.
- (44) Tissandier, M. D.; Cowen, K. A.; Feng, W. Y.; Gundlach, E.; Cohen, M. H.; Earhart, A. D.; Coe, J. V.; Tuttle, T. R. The Proton's Absolute Aqueous Enthalpy and Gibbs Free Energy of Solvation from Cluster-Ion Solvation Data. *J. Phys. Chem. A* **1998**, *102* (40), 7787–7794.
- (45) da Cunha, A. R.; Duarte, E. L.; Lamy, M. T.; Coutinho, K. Protonation/deprotonation process of Emodin in aqueous solution and pKa determination: UV/Visible spectrophotometric titration and quantum/molecular mechanics calculations. *Chem. Phys.* **2014**, *440*, 69–79.
- (46) Muckerman, J. T.; Skone, J. H.; Ning, M.; Wasada-Tsutsui, Y. Toward the accurate calculation of pKa values in water and acetonitrile. *Biochim. Biophys. Acta Bioenerg.* **2013**, *1827* (8), 882–891.
- (47) Park, S.; Choi, W.; Kim, S. H.; Lee, H.; Cho, K. Protonated Organic Semiconductors: Origin of Water-Induced Charge-Trap Generation. *Adv. Mater.* **2023**, *35* (42), 2303707.
- (48) Becke, A. D. Density-functional thermochemistry. III. The role of exact exchange. *J. Chem. Phys.* **1993**, *98* (7), 5648–5652.
- (49) Krishnan, R.; Binkley, J. S.; Seeger, R.; Pople, J. A. Self-consistent molecular orbital methods. XX. A basis set for correlated wave functions. *J. Chem. Phys.* **1980**, *72* (1), 650–654.
- (50) Marenich, A. V.; Cramer, C. J.; Truhlar, D. G. Universal Solvation Model Based on Solute Electron Density and on a Continuum Model of the Solvent Defined by the Bulk Dielectric Constant and Atomic Surface Tensions. *J. Phys. Chem. B* **2009**, *113* (18), 6378–6396.
- (51) Frisch, M. J.; Trucks, G. W.; Schlegel, H. B.; et al. *Gaussian 16*. Rev. C.01; Gaussian, Inc.: Wallingford, CT, 2016.